Journal of Molecular Structure 1237 (2021) 130313

Contents lists available at ScienceDirect

Journal of Molecular Structure

journal homepage: www.elsevier.com/locate/molstr

Highly effective aldose reductase mimetics: Microwave-assisted catalytic transfer hydrogenation of D-glucose to D-sorbitol with magnetically recoverable aminomethylphosphine-Ru(II) and Ni(II) complexes

Serhan Uruş[a,*], Hasan Eskalen[b], Mahmut Çaylar[a,c], Mehmet Akbulut[d]

[a] Chemistry Department, Faculty of Science and Letters, Kahramanmaraş Sütçü İmam University, 46050, Kahramanmaraş, Turkey
[b] Vocational School of Health Services, Department of Opticianry, Kahramanmaraş Sütçü İmam University, 46050 Kahramanmaraş, Turkey
[c] Research and Development Centre for University-Industry-Public Relations, Kahramanmaraş Sütçü İmam University, 46050, Kahramanmaraş, Turkey
[d] Materials Science and Engineering, Graduate School of Natural and Applied Sciences, Kahramanmaraş Sütçü İmam University, 46050, Kahramanmaraş, Turkey

ARTICLE INFO

Article history:
Received 11 September 2020
Revised 14 March 2021
Accepted 15 March 2021
Available online 22 March 2021

Keywords:
Aldose reductase
Catalysis
Nano
Phosphine
Sorbitol
Transfer hydrogenation

ABSTRACT

The novel Ru(II) and Ni(II) complexes of aminomethylphosphine ligands supported on Fe_3O_4@SiO_2 (core@shell) surface have been synthesized with Schlenk technique and characterized with Scanning Electron Microscopy (SEM), Energy-Dispersive X-Ray Spectroscopy (EDX), Transmission Electron Microscopy (TEM), X-Ray Diffraction Spectroscopy (XRD), Fourier-Transform Infrared Spectroscopy (FT-IR), Ultraviolet-Visible Spectroscopy (UV–Vis.), Thermogravimetric Analysis/Differential Thermal Analysis/ Differential Thermogravimetry (TG/DTA/DTG) and elemental analysis techniques. Besides, the synthesized complexes were tried as a catalyst in the transfer hydrogenation of D-glucose to D-sorbitol in isopropyl alcohol under microwave power at 150 °C for 1 h reaction time. K_2CO_3 was used as a base source in the catalysis. High-Performance Liquid Chromatography (HPLC) fitted Refractive Index Detector (RID) was used for the quantitative analyses of the catalytic tests. The complexes can be repeatedly usable and magnetically recoverable in the catalytic transfer hydrogenation of D-glucose to D-sorbitol. The complexes are also chemically selective and stable in the catalysis medium. In the recycling experiments, Ru(II) complexes were filtered and washed with isopropyl alcohol (IPA), dried and used again for the other catalytic cycles. Especially Ru(II) complexes showed the best catalytic properties, with over 91% selectivity on over 98% conversions under microwave power.

Introduction

There has been growing interest in synthesizing the metal complexes of phosphine derivatives since those are very active in various catalytic applications. Thus, the functionalized aminoalkylphosphines and their metal complexes are critical research areas for chemists. Ditertiary aminoalkylphosphines $(R_2PCH_2)_2NR$ćan be synthesized with the reaction of a phosphonium salt derivative $[R_2P(CH_2OH)_2]Cl$ and a primary amine $R'NH_2$ under N_2 atmosphere using the Schlenk technique. The chelated structured phosphine derivatives increase the stability and the catalytic reactivities of the metal complexes in the synthesis of many organic compounds [1,2,11-15,3-10]. Besides, the enantioselective organic products can be produced efficiently using a type of asymmetric aminophosphine-metal complex. The multidentate phosphine-metal complexes having excellent steric and electronic properties and π-back bonding properties can increase the catalytic efficiencies of the oxidation or reduction reactions. π-acceptor phosphine ligands can easily form π-back bonding with metal centers. Thus, these types of complexes can show unique catalysis properties and mechanisms. Because of these chemically flexible structures, the organic substrates and the reactive species can easily bond and change the molecular structure of the chelated metal-ligand complexes in the catalysis mechanism [6,16-23].

Fe_3O_4 (magnetite) nanoparticles have unique chemical and physical properties with having high surface area. Various inorganic-organic compounds can easily be bond onto the surface of Fe_3O_4 that gives excellent properties in many applications. Due to the unique chemical, physical and magnetic properties, the mag-

* Corresponding author.
E-mail address: serhanurus@yahoo.co.uk (S. Uruş).

https://doi.org/10.1016/j.molstruc.2021.130313
0022-2860/

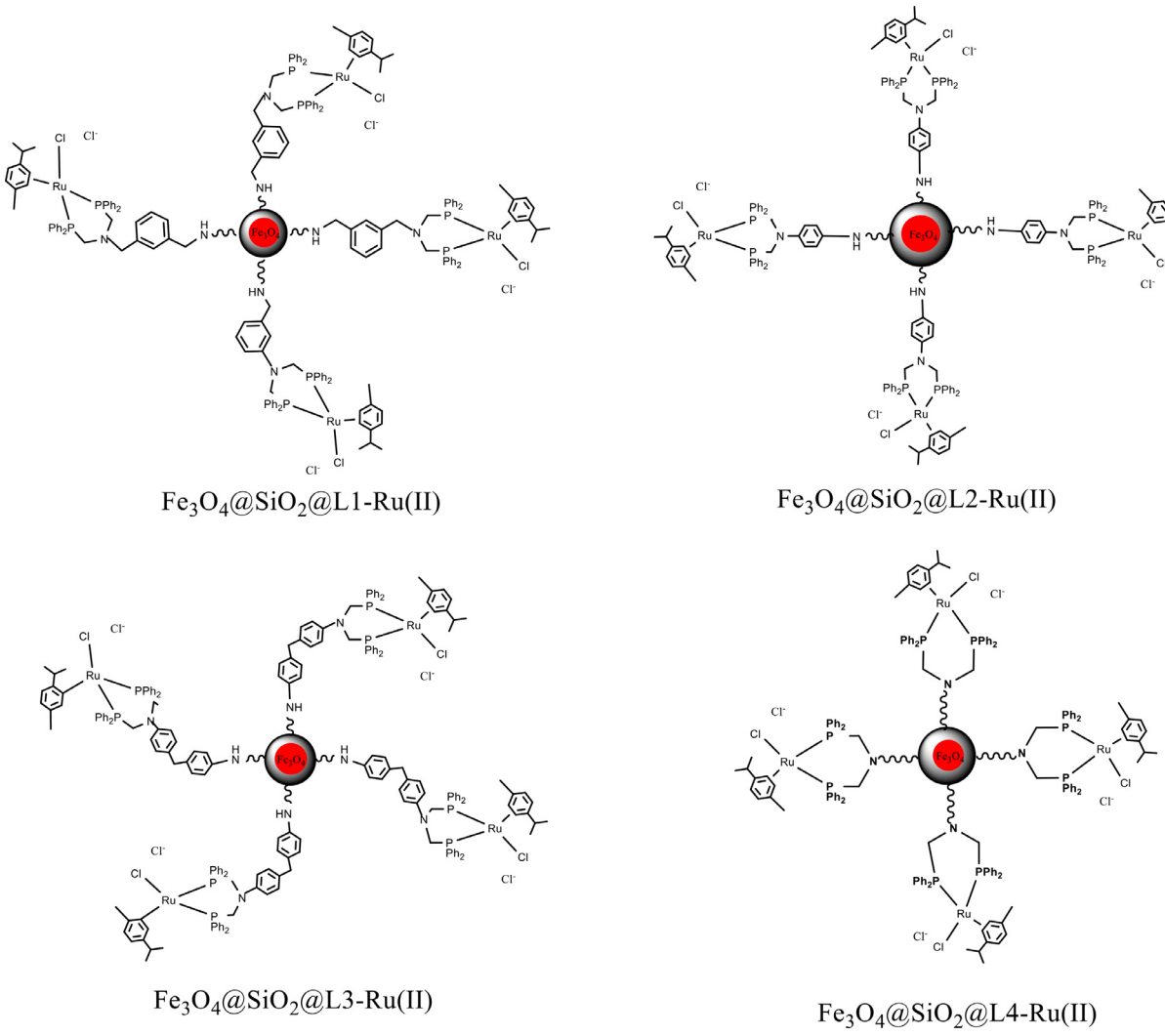

Fig. 1. Possible structures of the magnetite@silica supported aminomethylphosphine-Ru(II) e complexes.

netite nanoparticles can be used in chemical, physical, and biological applications. It can be used in medicine, such as, magnetic resonance imaging (MRI), and it can be used for the soil or water treatment from pollutants. Multifunctional nanomaterials can also show both optical and magnetic properties, due to their unique properties. For example, some nanocomposites can be used to imaging the real-time targeting fluorescence microscopy in blood vessels via control of the external magnetic field. The coating on the surface of magnetic-nano particles with silica provides unique advantages because of having excellent stability and activity in severe chemical and physical conditions. SiO_2 covering strengthens the nano-core structure in the severe chemical and physical conditions. Besides, if the silica surface is activated, the many types of ligands and the metal complexes can easily bond to the silica surface [23-32].

Sorbitol that annual production is over 700.000 tones/year is used in many different applications, like building blocks to synthesize fine chemicals such as ascorbic acid (intermediate in the synthesis of vitamin C). It is also used as an additive in the food, cosmetics, and paper industries. Sorbitol is also utilized as feedstock for hydrolysis-hydrogenation processes in order to produce isosorbide and useful polyols such as triols, tetrols, glycerol, ethylene glycol and 1,2-propanediol. Most of the sorbitol processing at an industrial scale is performed by catalytic hydrogenation of D-Glucose, a cheap raw material produced from starch and sucrose, using Raney-nickel catalysts. Both noble metals (Ru, Rh, Pd, and Pt) and non-noble metals (Fe, Ni, Cu, or Co) have been used as active phases in hydrogenation reactions. Nickel-based catalysts have achieved a good piece of attention according to their low cost and moderate to good catalytic activity.

Nevertheless, nickel-based catalysts are susceptible to show deactivation after recycling due to leaching of the active nickel into the reaction media, sintering of the active metal and poisoning of metallic nickel surface attributed to organic by products of the reaction. The current trend consists of the preparation of ruthenium-based catalysts, which show catalytic activities per-mass of active metal 20–50 times higher than nickel catalysts. However, the high price of noble metals is the main drawback. Thus, the development of novel bimetallic nickel-based catalysts with comparable high activity to noble metal catalysts still remains a technological challenge. Noteworthy efforts were carried out to enhance the catalytic activity of nickel-based catalysts in the catalytic conversion of D-Glucose into sorbitol [33,34,43-45,35-42].

In this study, the novel magnetically recoverable and repeatedly usable, selective and stable Ru(II) and Ni(II) complexes of aminomethylphosphine ligands supported on Fe_3O_4@SiO_2 surface have been synthesized and characterized. Especially, Ru(II) complexes showed the best catalytic acitivites over 91% selectivity on over 98% conversions using isopropyl alcohol in 1 h under microwave power.

Table 1
Important FT-IR vibration modes.

	FT-IR (cm^{-1})							
Compound	OH/NH	ArC–H	RC–H	ArC=C	P-Ph/C–N	Si-O	M-P	M-Cl
L1	3409	3000	2889	1623	1425	1069	–	–
L2	3402	2916	2928	1610	1420	1066	–	–
L3	3411	2986	2905	1608	1423	1065	–	–
L4	3404	2995	2870	1629	1420	1063	–	–
L1-Ru(II)	3198	3012	2895	1623	1405	1049	545	439
L2-Ru(II)	3227	2954	2890	1624	1405	1051	549	440
L3-Ru(II)	3195	2988	2902	1621	1405	1048	541	431
L4-Ru(II)	3337	3975	2895	1624	1395	1059	539	436
L1-Ni(II)	3357	2920	2895	1624	1410	1099	532	446
L2-Ni(II)	3354	2979	2901	1630	1391	1066	537	440
L3-Ni(II)	3333	2978	2887	1630	1387	1060	541	416
L4-Ni(II)	3371	2989	2892	1624	1393	1060	541	420

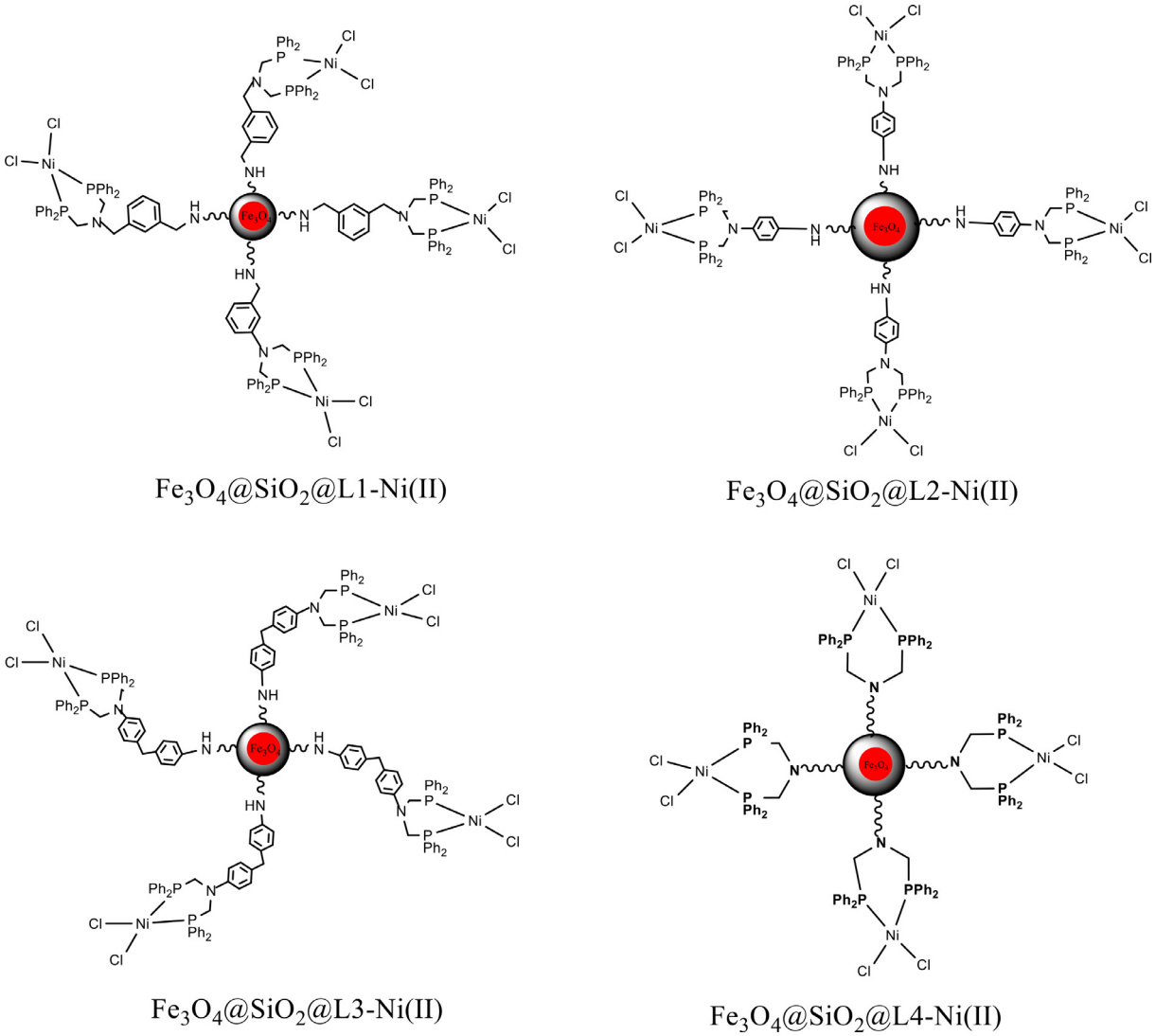

Fig. 2. Possible structures of the magnetite@silica supported aminomethylphosphine-Ni(II) complexes.

2. Experimental

2.1. Characterization techniques

FT-IR spectra were obtained using KBr pellets on Perkin-Elmer Spectrum 400 system in the range 4000–400 cm^{-1}. The thermal properties of the ligands were investigated on a SII thermal system under a nitrogen atmosphere at a heating rate of 10 °C /min in the range 30–1000 °C. The surface morphology and EDX analysis of the nanocomposite ligands and their complexes were evaluated using Zeiss Evo LS10 SEM attached with Bruker Quantax EDS. TEM images were taken with the Hitachi HT7700 instrument. X-ray diffraction (XRD) patterns were recorded on the PANalytical Xprt pro. UV-Visible reflectance spectra were recorded at solid state using Hitachi U-3900 Spectrophotometer attached with solid state reflectance apparatus. The microwave syntheses were done in

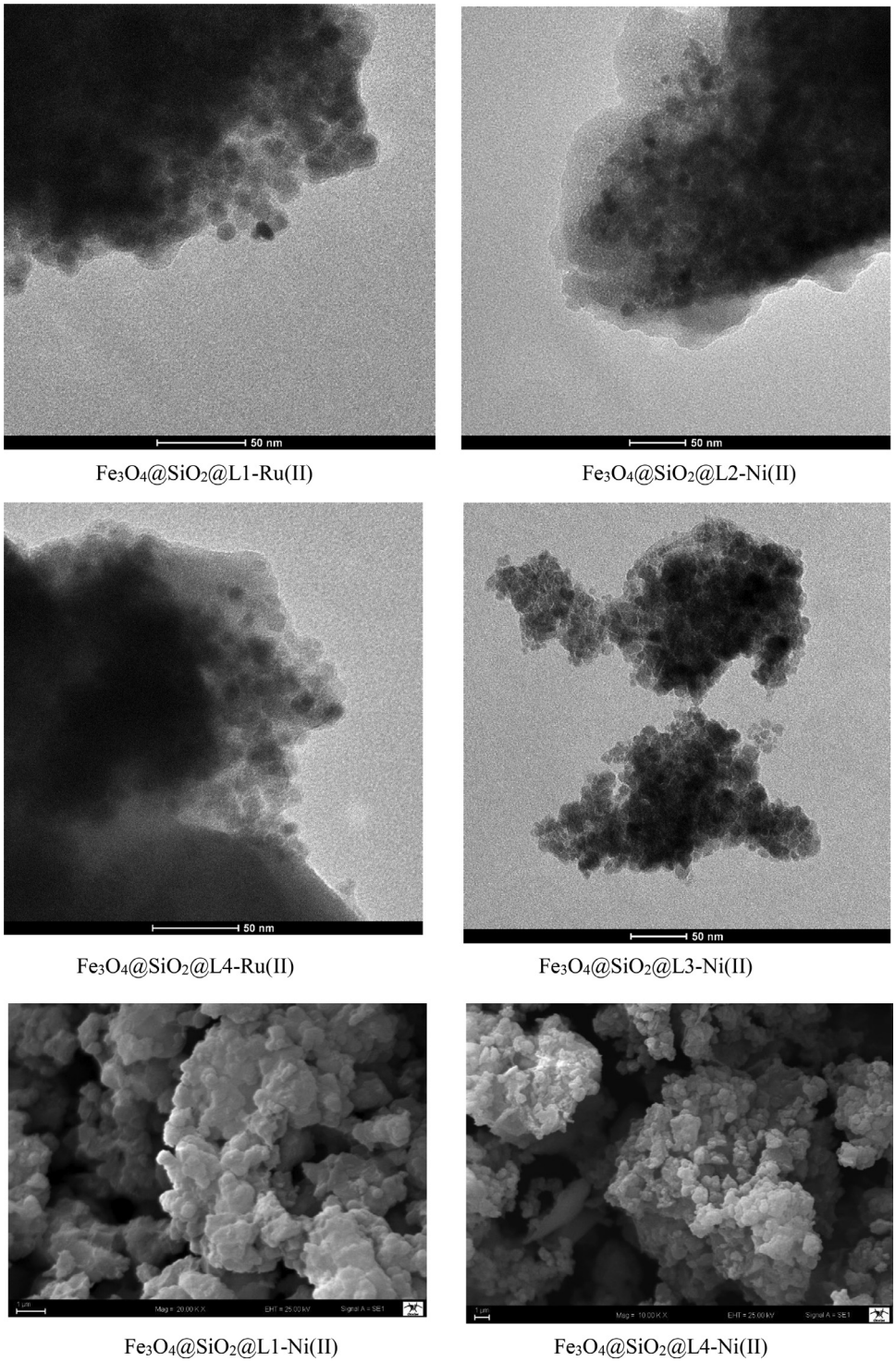

Fig. 3. TEM and SEM images of the complexes.

quartz vessels closed with teflon covers using the Milestone Start-Synth instrument with temperature control. Shimadzu HPLC LC-20AD, HPLC fitted with Inertsil NH_2 column and RID-10A was used for the catalytic experiments. Calibration standards of D-glucose, D-sorbitol, D-mannitol and D-fructose were prepared in acetonitrile and injected into HPLC. External calibration curves were drawn by the instrument software with the obtained data for all sugars. This system was controlled, and data processed, with Prominence software. The separation was achieved on a Carbosep Coregel Inertsil NH_2 column (300 × 7.8 mm). All samples and standards were passed through PVDF 0.45 μm syringe filters (Teknokroma) prior to injection. Each run was completed within 30 min.

2.2. Synthesis of Ru(II) and Ni(II) complexes of magnetite-silica supported aminomethylphosphine ligands

$Fe_3O_4@SiO_2(CH_2)_3NHRN(CH_2PPh_2)_2$ type aminomethylphosphine ligands were synthesized according to our previous study [23]. Firstly, 2 mmol $FeCl_3{\bullet}6H_2O$ (0.5516 g, 98%), 10 mmol NaOAc (0.8286 g, 99%) and 2 mmol Na_3Cit (0.5912 g, 99.5%) were

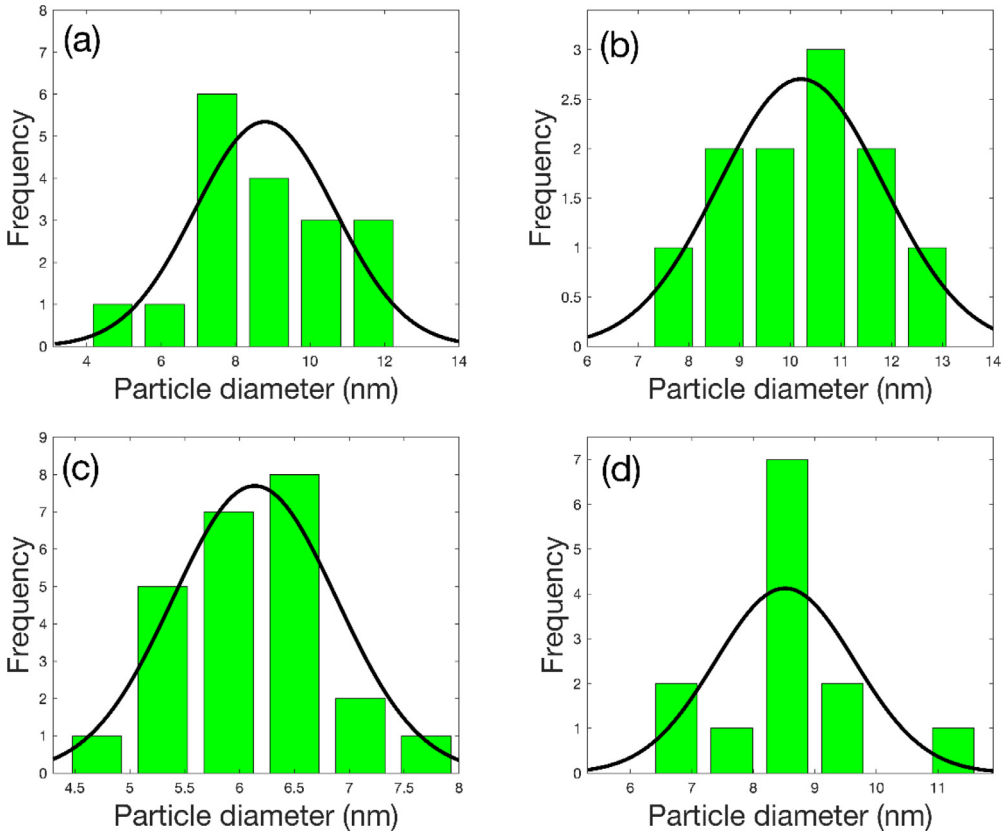

Fig. 4. The particle size distribution histograms of the selected complexes
a: Fe_3O_4@SiO_2@L1-Ru(II), b: Fe_3O_4@SiO_2@L1-Ni(II), c: Fe_3O_4@SiO_2@L3-Ni(II), d: Fe_3O_4@SiO_2@L4-Ru(II).

dissolved in 20 mL ethylene glycol in the quartz tube of the microwave oven and stirred for 1 h at room temperature. The color of the solution changed from yellow to red. The second and the shorter microwave process improved by us; the quartz tube was closed with teflon cover and microwaved at 200 °C for 1 h with power controlled instrument set to max. 600 watt. The obtained magnetic nano-core Fe_3O_4 was filtered and washed with EtOH and dried at 60 °C for 12 h. In the second, 0.5 g nano Fe_3O_4 was dispersed in 100 mL EtOH for 10 min in the ultrasonic bath, 5 mL NH_3 solution (26%) was added to this dispersion and stirred for 15 min. 0.5 mL Triton X-100 and 10 mL tetraethyl orthosilicate (TEOS) was dropped to final dispersion and stirred for 12 h at room temperature. The obtained Fe_3O_4@SiO_2 was filtered and washed with EtOH: H_2O (1:1) solution. Thirdly, 0.5 g obtained Fe_3O_4@SiO_2 nanocomposite was added to in the appropriate amount of toluene and ultrasonicated for 10 min. This solution was treated with 5 mmol (3-aminopropyl)triethoxysilane (APTES) (1.18 mL, 99%) and refluxed for 12 h. The obtained amino-substituted nanocomposite was filtered and washed with EtOH and diethyl ether. The precipitation was dried at 60 °C for 12 h. Finally, 0.5 g obtained Fe_3O_4@SiO_2 nanocomposite was added to an appropriate amount of toluene and ultrasonicated for 10 min. This solution was treated with 5 mmol (3-chloropropyl)triethoxysilane (APTES) (1.27 mL, 95%) and refluxed for 12 h under nitrogen atmosphere. The obtained chloro–substituted nanocomposite was filtered and washed with EtOH and diethyl ether. The precipitation was dried at 60 °C for 12 h.

0.25 g Fe_3O_4@SiO_2@$OSi(CH_2)_3NHRNH_2$ type primary amine was dispersed in 25 mL EtOH. 2 mmol phosphonium salt $[PPh_2(CH_2OH)_2]Cl$ and 1 mL NEt_3 was added to this solution and refluxed for 90 min under a nitrogen atmosphere using vacuum manifold in Schlenk flask. After that, the liquid phase was decantated while the solid phase was kept using a magnet. The precipitation was washed with three portions of EtOH. 1 mmol (0,6313 g) $[Ru(p\text{-}cymene)Cl_2]_2$ and 2 mmol (0,2592 g) $[NiCl_2]$ was added to each of the obtained Fe_3O_4@$SiO_2(CH_2)_3NHRN(CH_2PPh_2)_2$ type magnetic nano-composite supported aminomethylphosphine ligands dispersed in 25 mL EtOH. The mixture was refluxed for 6 h under a nitrogen atmosphere. The obtained nanocomposite supported bis(diphenylphosphinomethyl)aminoalkyl-Ru(II) and Ni(II)

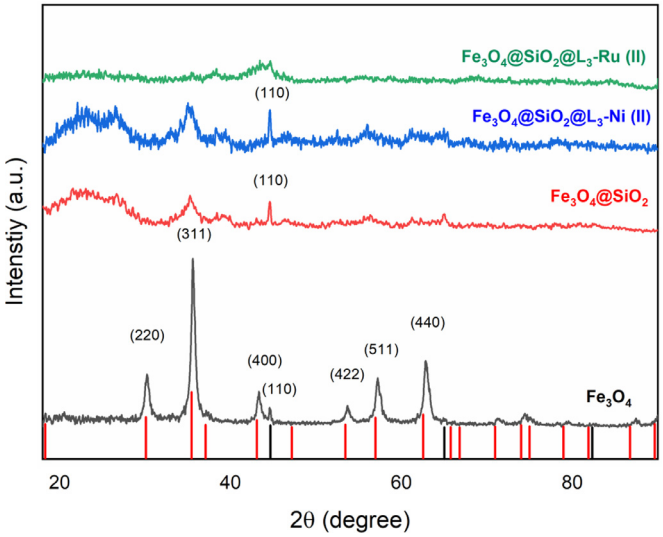

Fig. 5. XRD patterns of Fe_3O_4, Fe_3O_4@SiO_2, Fe_3O_4@SiO_2@L3-Ni(II) and Fe_3O_4@SiO_2@L3-Ru(II) complexes.

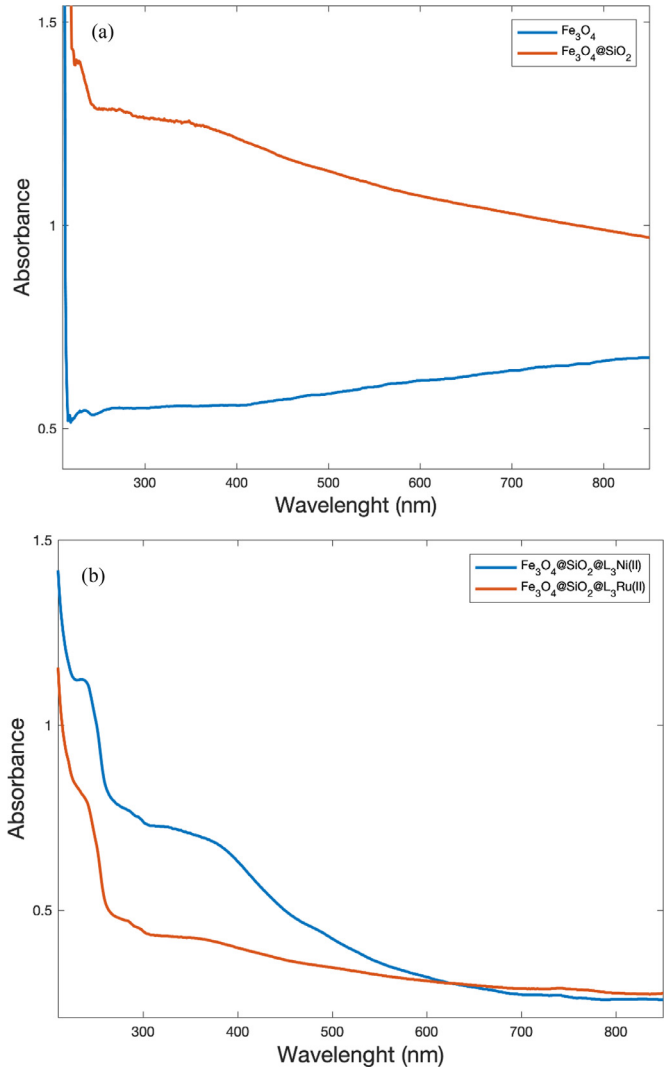

Fig. 6. UV–Vis. spectra of the synthesized compounds.

complexes were filtered and washed with EtOH. The precipitations were dried at 60 °C for 12 h. The proposed chemical structures of the complexes are given in Fig. 1 and 2.

2.3. Catalytic synthesis of D-Sorbitol from D-Glucose with transfer hydrogenation

In the optimized catalytic process, 0.1 g nano-catalyst was ultrasonicated in 10 ml of isopropyl alcohol (99.4%) in a quartz tube of the microwave oven. Then, 1 mmol of D-(+)-glucose monohydrate in 15 ml of distilled water and 0.1 mmol of K_2CO_3 was added, respectively and the microwave program was applied in the closed system. Microwave oven program; starting from ambient temperature to 150 °C for 20 min and treated at 150 °C for 40 min set to max. 600 watt. Then, it is left to cool down in 15 min. After the reaction, 200 µL of the mixture was taken from the quartz and diluted to 2 mL with distilled water. The diluted mixture was passed through a 0.45-micron filter, and 20 µl mixture was injected into HPLC. The conversions and the selectivities were calculated from the external calibrations of D-glucose, D-mannitol, D-fructose and D-sorbitol.

HPLC Experimental Conditions:

Module	Conditions
Pump	Mobile phase acetonitrile: water (70:30%)Flow rate: 0.5 ml/min
Autosampler	Injection volume: 20 µl
Oven	Temperature: 35 °C
Detector	Refractive index (+)
Column	Inertsil NH_2

3. Results and discussion

3.1. Characterization

3.1.1. Thermal analyses

Aminomethylphosphine-Ru(II) and Ni(II) complexes supported on Fe_3O_4@SiO_2 nanocomposite behaved the similar thermogravimetric properties as seen in Figure S1. All the complexes showed four endothermic degradation bands in TG/DTA/DTG curves. Firstly, the adsorbed water molecules were desorbed from the ambient temperature to 90 °C. The dissociation of silanol groups and chloro ligands degraded to about 300 °C with an endothermic band. Aminophosphine and p-cyemene ligands having aromatic and the aliphatic substituents decomposed to over 600 °C with an endothermic band. The last band was due to the formation of metal-oxides. The total degradations of the complexes were 15–20%. Fe_3O_4, SiO_2, and metal-oxide derivatives have arisen after the temperature program.

3.1.2. Morphology

Non-uniform spherical structures were observed in TEM and SEM images of Fe_3O_4-supported aminomethylphosphine-Ru(II) and Ni(II) complexes. It can be said that silica was covered on the spherical magnetite particles. The diameter of the supported complexes on the spherical particles have about 10 nm (Fig. 3). The diameter of Fe_3O_4@SiO_2@L3-Ni(II) complex particle calculated as 6.14 nm ± 0.75 nm for Fe_3O_4@SiO_2@L3-Ni(II) (Fig. 4).

3.1.3. EDX

The EDX spectra of the synthesized Fe_3O_4@SiO_2@aminomethylphosphine-Ru(II) and Ni(II) complexes were confirmed the complexation on the nanocomposite surface having phosphorus, carbon, nitrogen, oxygen, iron, silicon, chlorine and the metal for each complex. (Figure S2).

3.1.4. XRD analyses

In order to study the crystalline structural properties and phase information of the synthesized Fe_3O_4@SiO_2 based aminomethylphosphine-metal complexes, X-Ray diffraction analyses were conducted. The XRD patterns for Fe_3O_4, Fe_3O_4@SiO_2, Fe_3O_4@SiO_2@L3-Ru(II) and Fe_3O_4@SiO_2@L3-Ni(II) were given in Fig. 4. The graphic explicitly demonstrates both the crystalline and amorphous structures formation. The highest crystalline structures obtained for Fe_3O_4 nano-particles with obvious six peaks at around 2θ angle of 30.10°, 35.42°, 43.12°, 53.65°, 56.96° and 62.52 correspondings to the (220), (311), (400), (422), (511) and (440) crystal planes of the Fe_3O_4 (Ref. Code. 01–075–1610, PDF2 database) similarly also found in recent literature [46,47]. In the illumination of the XRD results, the cubic structure of Fe_3O_4 nanoparticles is synthesized. The crystalline size of the nanoparticles was found by utilizing the Scherrer formula determined as 44.3 nm. There is also a small peak around 44.67 related to the cubic form of iron (Ref. Code: 01–087–0721). The bottom lines demonstrate the reference card bars of Fe_3O_4 and Fe with red and black color, respectively. The XRD pattern of Fe_3O_4@SiO_2 nanocomposite decreases the intensity of Fe_3O_4 diffraction pattern that indicates the existence of the disordered structure of Fe_3O_4@SiO_2 nano-particles [48]. The diffraction pattern of Fe_3O_4@SiO_2@L3-Ni(II) composite is given in green in Fig. 5, with introducing aminomethylphosphine-Ni(II)

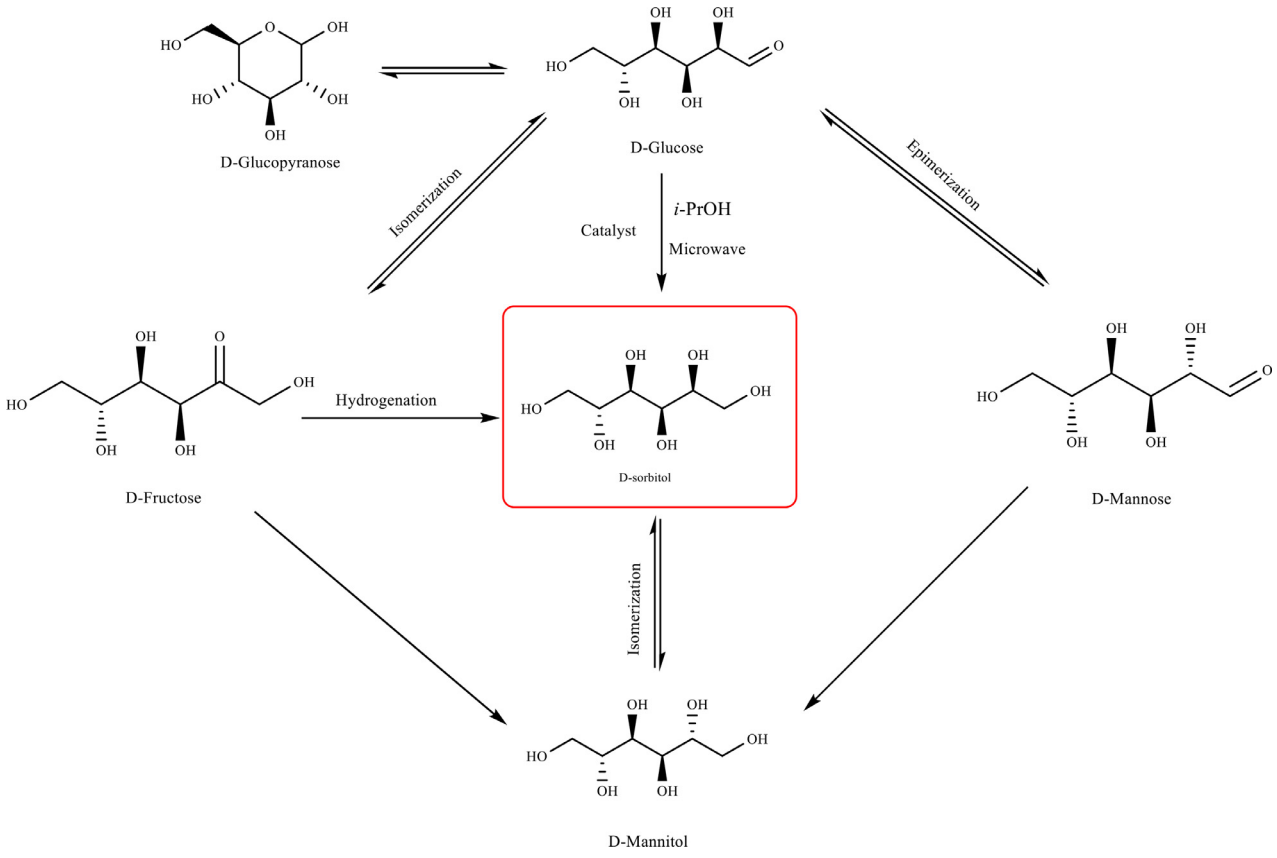

Fig. 7. Hydrogenation of D-glucose [59].

complex to Fe_3O_4@SiO_2 composites, the pattern slightly changed. The most apparent peak centered at 44.67° indicates iron phase. Also, for Fe_3O_4@SiO_2-L3-Ru(II) complex, the crystalline peak at 44.67° and 64.98° represents the existence of iron phase.

3.1.5. Optical absorption analyses

The metal-to-ligand charge-transfer (MLCT) transitions of the complexes were observed at around 360 nm due to the π-acidity of phosphorus-carbon σ^*−antibonding orbitals in aminomethylphosphine ligands in the metal complexes. Thus, these type of the ligands are known as σ-donors and strong π-acceptors [23,49,50]. MLCT transfer bands were seen in UV spectra of Fe_3O_4@SiO_2@bis(diphenylphosphinomethyl)amine-Ni(II) and Ru(II) complexes. Besides, the forbidden D-d-d transitions of the complexes were recorded at around 485 nm as very small bands [23, 49, 50].

3.1.6. FT-IR

The band gap of the synthesized nanocomposites was calculated by using the Tauc equation;

$$(Ah\upsilon)^n = B(h\upsilon - E_g)$$

here, E_g is optical band gap of the composites, hv is the photon energy, B is material constant, A is the amount of absorbance and n is constant depends on the material. The selected UV–Vis. spectra and the calculated band gaps of all the synthesized complexes were given in Fig. 6 and Fig. S3. The graphics of band gap energies of the synthesized nanoparticles under the light of the above mentioned studies were plotted as seen Fig. S3 [51-55].

The band gap values of Fe_3O_4 were reported as 2.04 eV in the literature [56], but in our study, we found band gap of Fe_3O_4 as 2.08 eV. The band gap increased by introducing SiO_2 to 2.31 eV was found in this study. The calculated band gaps were given in Figure S2 and band gap values for Fe_3O_4@SiO_2@L1-Ni(II) and Fe_3O_4@SiO_2@L4-Ru(II) was calculated as 2.37 eV and 2.38 eV respectively.

3.1.6. FT-IR spectra

Silica peaks from the covering on the magnetite in the complexes were impressed to the vibration modes of the functional groups in FT-IR spectra. The silanol-OH and secondary amine N–H stretching modes of the magnetite@SiO_2 supported aminomethylphosphine-metal complexes were overlapped with a wide band at about 3100–3400 cm^{-1}. Aromatic and aliphatic C–H stretching modes were recorded at around 3000–2890 cm^{-1}. Aromatic $C = C$ stretching mode was seen at around 1620 cm^{-1}. The wideband around 1060 cm^{-1} was because of Si-O asymmetric stretching modes. P-Ph and C-N stretch of the supported aminomethylphosphine-metal complexes were collected as one broad peak at about 1400 cm^{-1}. Besides, M-P and M-Cl vibration modes of the complexes were collected about 530 $cm^{-1}$and 430 cm^{-1} in FT-IR spectra of the complexes (Table 1 and Figure S4).

3.2. Catalytic synthesis of D-Sorbitol by D-Glucose transfer hydrogenation: aldose reductase mimetics

The novel synthesized nanocomposite supported, magnetically recoverable aminomethylphosphine-Ru(II) and Ni(II) complexes were used in the transfer hydrogenation of D-glucose to D-sorbitol in isopropyl alcohol under microwave power in 1 h reaction time. Isopropyl alcohol (i-PrOH) is used as a solvent and hydrogen source in the transfer hydrogenation reactions, which is cheap, safe, nontoxic, environmentally friendly [57]. All the novel Ru(II) complexes showed outstanding catalytic activities, especially Fe_3O_4@SiO_2@L_2-Ru(II) complex was the best at 97.18% selectivity with 99.11%

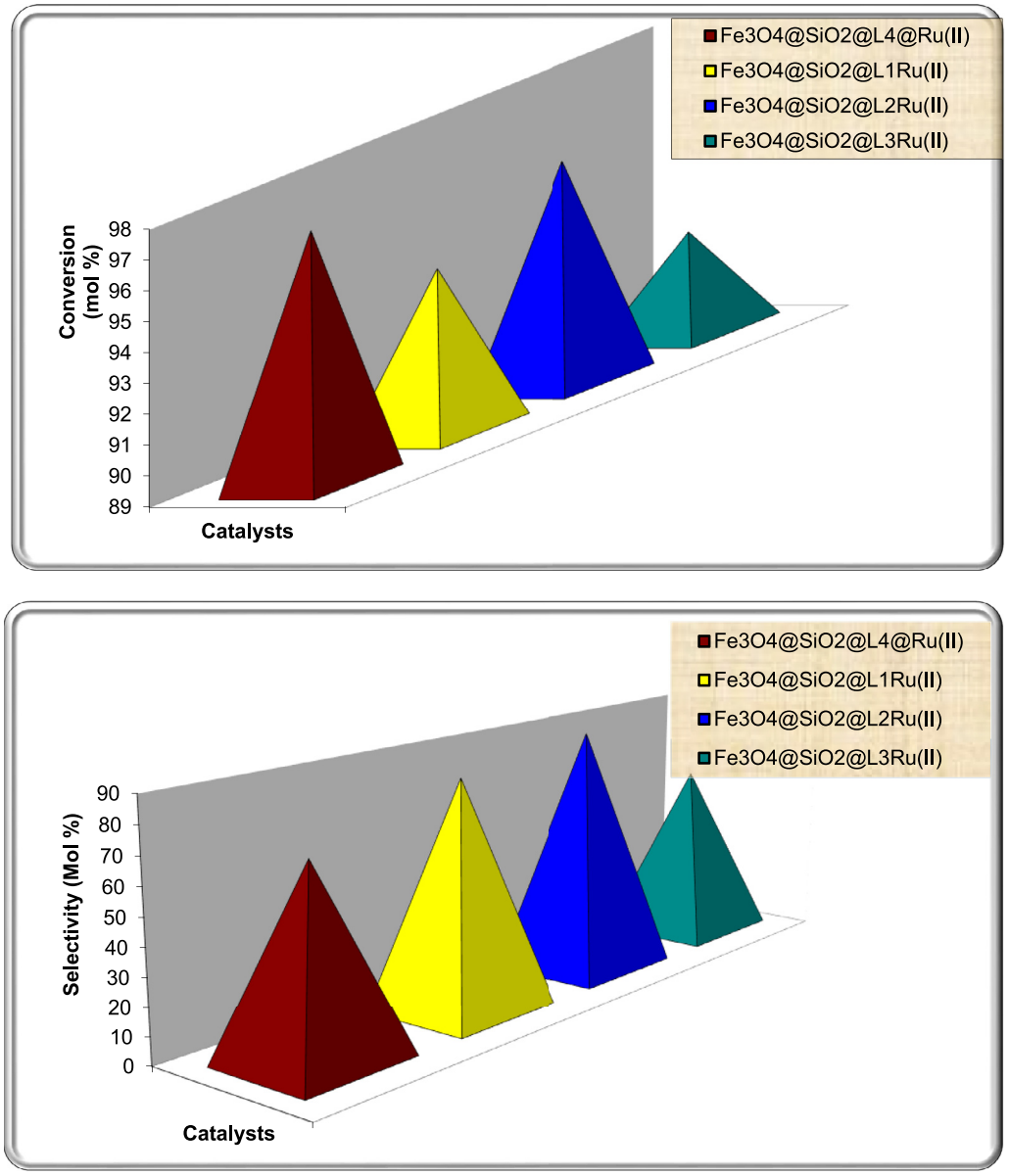

Fig. 8. Conversions and selectivities for Ru(II) complexes.

Table 2
Conversions and selectivities for the aldose reductase mimetics.

Catalyst	Conversion (mol%)	Selectivity (mol%)
Fe_3O_4@SiO_2@L1-Ru(II)	98,28	94,45
Fe_3O_4@SiO_2@L2-Ru(II)	99,11	97,18
Fe_3O_4@SiO_2@L3-Ru(II)	97,18	95,29
Fe_3O_4@SiO_2@L4-Ru(II)	98,15	91,25
Fe_3O_4@SiO_2@L1-Ni(II)	97,80	58,17
Fe_3O_4@SiO_2@L2-Ni(II)	98,10	55,37
Fe_3O_4@SiO_2@L3-Ni(II)	96,25	56,54
Fe_3O_4@SiO_2@L4-Ni(II)	97,15	68,89

conversion when compared to the literature in the route of the transfer hydrogenation of D-glucose to D-sorbitol [36,37,40,58-63]. Fe_3O_4@SiO_2@L_2–Ni(II) complex was also very active in the transfer hydrogenation of D-glucose to D-sorbitol over 68.89% selectivity with 97.15% conversions (Fig. 8, 9, Table 2) (chromatograms given in each catalyst in supplementary as separate pdf files). According to the possible catalytic reaction mechanism (Fig. 7) and the literature, catalysis is very important for the transfer hydrogenation of D-glucose to D-sorbitol working as a brain in the reaction. The high selectivities can be obtained by using a catalyst in the transfer hydrogenation [36,37,40,58-63].

The nano-core magnetite (Fe_3O_4) is a unique supporting material because of its large area and its magnetic properties for the silica gel's controlly precipitation. In addition, covering of SiO_2 on a nano-core provides additional vital features because of its unique chemically and physically stability in severe chemical and physical conditions for the catalyst supporting. Ru(II) complexes of aminomethylphosphine ligands supported on Fe_3O_4@SiO_2 calculated small band gap like a semiconductor (Figure S3) gives unique properties in the transfer hydrogenation of D-glucose to D-sorbitol due to the electron transfer from i-PrOH (reducing agent) to metal center and finally to the substrate in the possible mechanism. In addition, nanocomposite supported complexes having about 2.0–2.5 eV band gaps supply an easy electron circulation from the substrates to the reducing agent (i-PrOH). Also, the effect of the microwave excitation to the bonds provides a large positively charged surface area for the binding of substrates and the re-

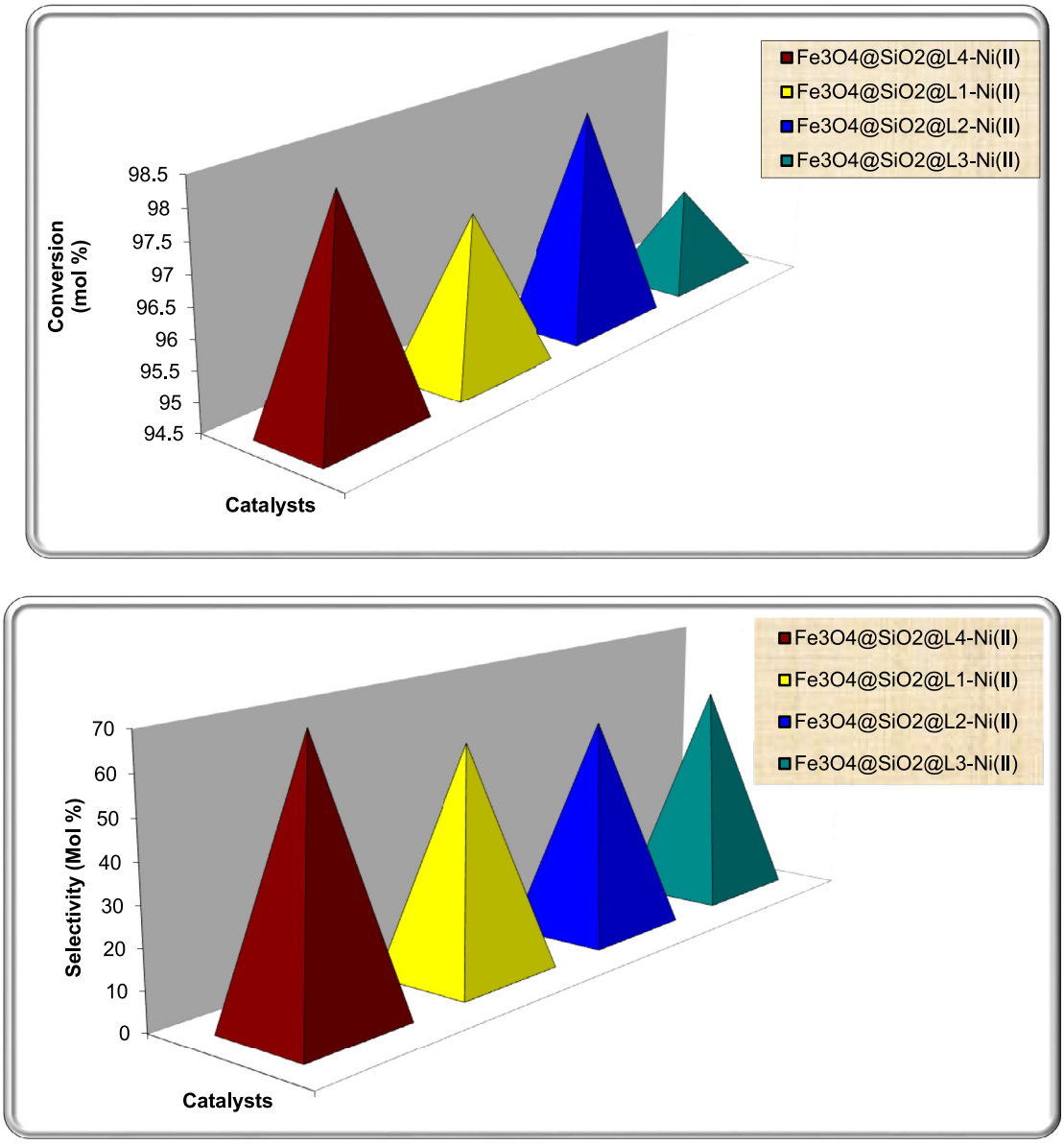

Fig. 9. Conversions and selectivities for Ni(II) complexes.

ducing agents with a complexation in the reaction possible mechanism (Fig. 10). Aminomethylphosphine ligands have excellent steric and electronic properties that can increase the catalytic transfer hydrogenation activity because of having π-back bonding properties in the metal complexes. π-acceptor aminomethylphosphine ligands can form π-back bonding with metal centers, and they can play unique catalytic activities in the catalysis mechanism. Because the strong π-back bonding in the complex can facilitate the leaving of chloro and p-cymene ligands, and then formed D-glucose-Ru(II)-aminomethylphosphine-(i-PrOH) pre-complexes in the effect of K_2CO_3 base. In the activated Ru(II) complexes, having coordinated the sugar substrate and the reducing agent can easily change the molecular structure of the chelated metal-ligand complexes in the proposed catalysis mechanism. The hydrogen transfer from i-PrOH to the carbonyl group of glucose in the coordination sphere can be formed and then acetone and D-sorbitol leaves from the metal center (Fig. 5) [6,16,34,35,57,59,64,17-23,33].

The microwave power in the closed reactor system increased D-sorbitol selectivity with Ru(II) catalyst while controlling the oxidizing to gluconolactone and rearrangement and isomerization of D-glucose to D-mannitol and D-fructose in the transfer hydrogenation reaction mechanism like a processor. Additionally, the microwave irradiation in the closed system provided the bond activation of sugar having dipole fields with the homogeneous heating resulted in the transfer of hydrogen from isopropyl alcohol to D-glucose efficiently. Thus, it was obtained 97.18% selectivities with 99.11% conversions that is the best in the literature [35,38,40,58,62,63,65].

The Ru (II) complexes were removed from the reaction medium with a magnet and washing after each analysis, and re-usability was examined in the cycles. The Ru(II) complexes, which have the highest recovery in five cycles, especially Fe_3O_4@ SiO_2@L2-Ru (II) complex (Table 3, Fig. 11).

Conclusions

In the study, Fe_3O_4@SiO_2 supported-bidentate ditertiary aminomethylphosphine ligands and their Ru(II) and Ni(II) complexes have been synthesized using the Schlenk technique under nitrogen atmosphere. The synthesized complexes were tried as aldose reductase mimetics in the transfer hydrogenation of D-

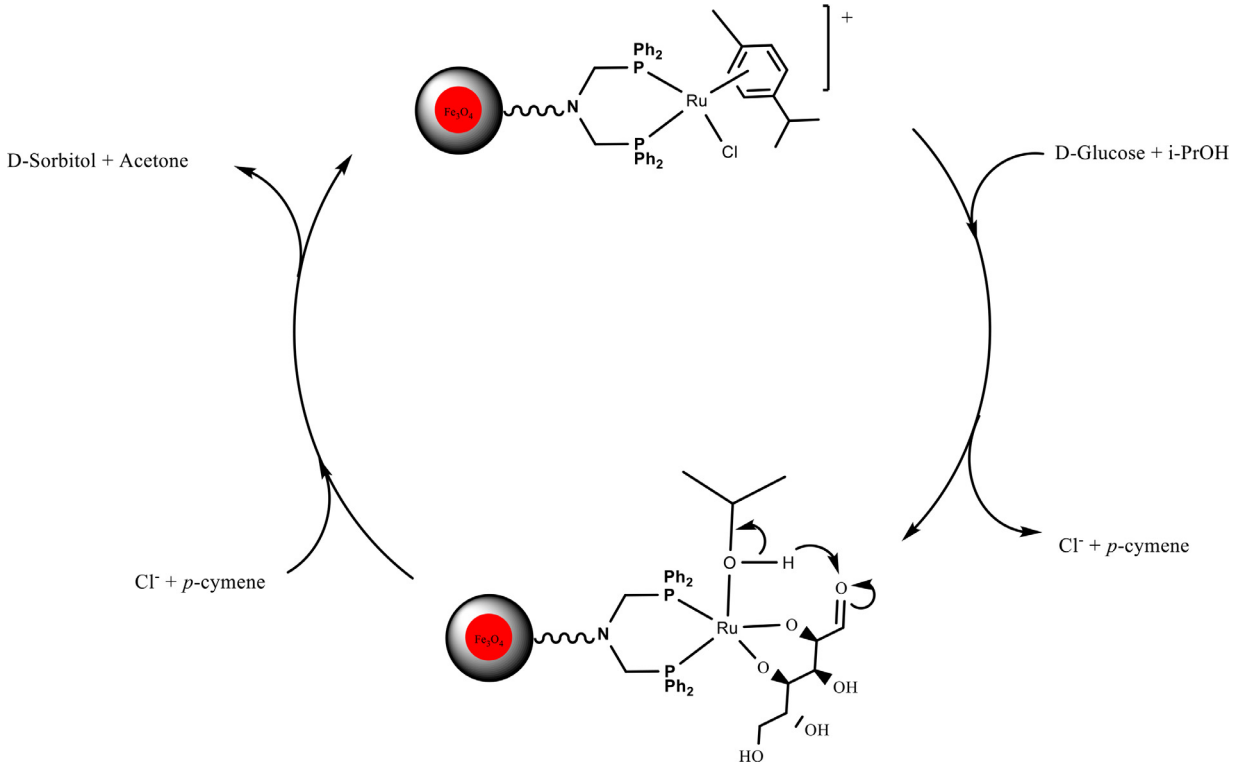

Fig. 10. Possible mechanism of transfer hydrogenation of D-glucose.

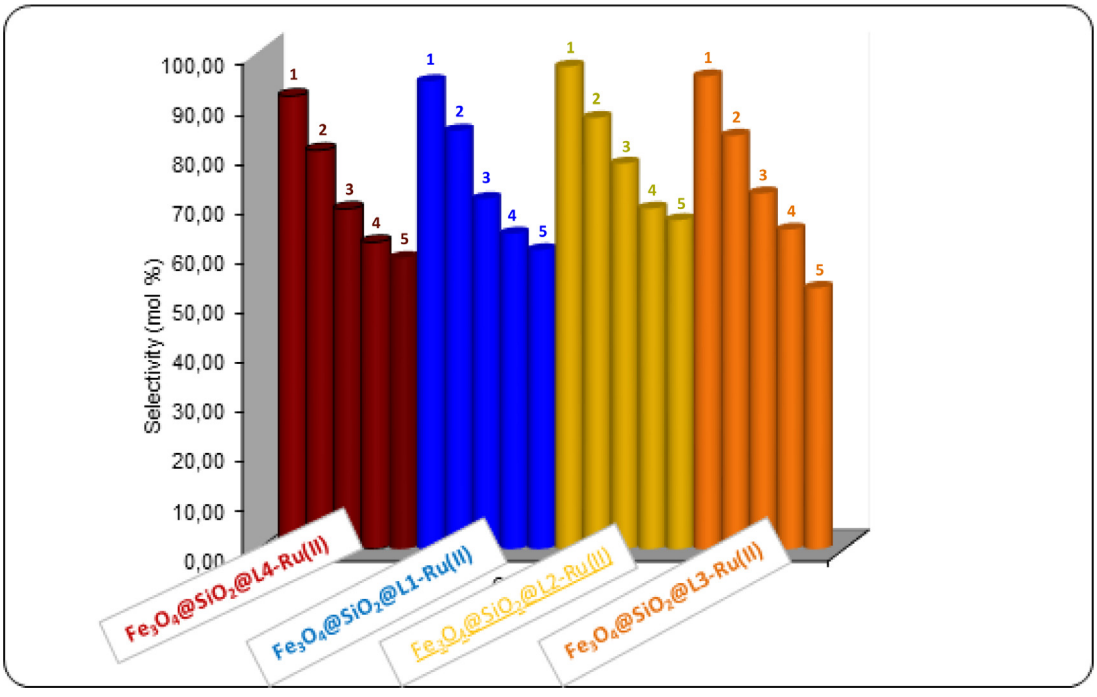

Fig. 11. Recycling graphics for Ru(II) complexes.

Table 3
Catalytic Recycles of Ru(II) Complexes.

Catalyst	Catalytic Recycles				
	1	2	3	4	5
Fe_3O_4@SiO_2@L1-Ru(II)	94,45	84,10	70,40	63,40	60,10
Fe_3O_4@SiO_2@L2-Ru(II)	97,18	86,68	77,50	68,45	66,10
Fe_3O_4@SiO_2@L3-Ru(II)	95,29	83,10	71,50	64,20	52,50
Fe_3O_4@SiO_2@L4-Ru(II)	91,25	80,20	68,40	61,70	58,50

glucose to D-sorbitol in the closed microwave system. The Ru(II) complexes showed the best selectivities by using K_2CO_3 in i-PrOH. The best conversions and the selectivities were obtained in 1 h compared to the literature. The excellent chemical properties of the aminomethylphosphine-Ru(II) complexes with the effect of the microwave power in the closed reactor system and the electron mobility of the nanocomposite surface a semiconductor increased the catalytic activities of showed a unique catalytic property. The

obtained selectivities and the conversions are the best in the literature.

Credit author statement

Serhan URUŞ: Synthesis, characterization, catalysis
Hasan ESKALEN: XRD, band gap
Mahmut ÇAYLAR: Synthesis, catalysis
Mehmet AKBULUT: Synthesis, catalysis

Declaration of Competing Interest

The authors declare that they have no known competing financial interests or personal relationships that could have appeared to influence the work reported in this paper.

Acknowledegements

We would like to thank Kahramanmaraş Sütçü İmam University (Project No: 2018/2–2 YLS) for the financial supports.

Supplementary materials

Supplementary material associated with this article can be found, in the online version, at doi:10.1016/j.molstruc.2021.130313.

References

[1] Ö. Sariöz, S. Öznergiz, Synthesis and characterizaton of monoaminophosphine, bis(amino)phosphine derivatives, and their metal complexes, Synth. React. Inorganic, Met. Nano-Metal Chem. 41 (2011) 698–703, doi:10.1080/15533174.2011.568464.
[2] O. Serindag, Synthesis of some platinum(II) diphosphine complexes of the type [PtX2(P-P)] (X2 = CO3; X = CH3COO, CF3COO, NCO), Synth. React. Inorg. Met. Chem 27 (1997) 69–76, doi:10.1080/00945719708000183.
[3] O. Serindag, M. Keles, Synthesis of some nickel(II) diphosphine complexes having coordinated carboxylates, Synth. React. Inorganic, Met. Nano-Metal Chem. 38 (2008) 580–583, doi:10.1080/15533170802293238.
[4] M. Keles, Z. Aydin, O. Serindag, Synthesis of palladium complexes with bis(diphenylphosphinomethyl)amino ligands: a catalyst for the Heck reaction of aryl halide with methyl acrylate, J. Organomet. Chem. 692 (2007) 1951–1955, doi:10.1016/j.jorganchem.2007.01.003.
[5] M. Keleş, T. Keleş, O. Serindağ, Palladium complexes with bis(diphenylphosphinomethyl)amino ligands and their application as catalysts for the Heck reaction, Transit. Met. Chem. 33 (2008) 717–720, doi:10.1007/s11243-008-9101-z.
[6] P.E. Garrou, Transition-metal-mediated phosphorus-carbon bond cleavage and its relevance to homogeneous catalyst deactivation, Chem. Rev. 85 (1985) 171–185, doi:10.1021/cr00067a001.
[7] P.E. Garrou, Ring contributions to the phosphorus-31 chemical shifts of transition metal-phosphorus chelate complexes, Inorg. Chem. 14 (1975) 1435–1439, doi:10.1021/ic50148a055.
[8] L. Ortego, J. Gonzalo-Asensio, A. Laguna, M.D. Villacampa, M.C. Gimeno, Aminophosphane)gold(I) and silver(I) complexes as antibacterial agents, J. Inorg. Biochem. 146 (2015) 19–27, doi:10.1016/j.jinorgbio.2015.01.007.
[9] S. Uruş, M. Keleş, O. Serindağ, Synthesis of silica-supported Platinum(II) and nickel(II) complexes of bis(Diphenylphosphinomethyl)amino ligand: applications as catalysts for the synthesis of 2-Methyl-1,4-Naphthoquinone (vitamin K 3), J. Inorg. Organomet. Polym. Mater. 20 (2010) 152–160, doi:10.1007/s10904-010-9328-y.
[10] M. Dolaz, S. Uruş, G. Ceyhan, Synthesis, Characterization and Catalytic Properties of Benzylphosphonate-aminethylphosphine-Pd(II), Cu(II), Ru(II) and V(IV) Complexes, J. Inorg. Organomet. Polym. Mater. 29 (2019) 1575–1586, doi:10.1007/s10904-019-01121-3.
[11] S. Uruş, M. İncesu, S. Köşker, A.H. Kurt, G. Ceyhan, Synthesis, characterization, photoluminescence and electrochemical properties of Pt(II) and Ag(I) complexes of tetradentate aminomethylphosphine ligands and antiproliferative activities on HT-29 human colon cancer, Appl. Organomet. Chem. (2017) 31, doi:10.1002/aoc.3550.
[12] S. Uruş, H. Adıgüzel, M. Keleş, İ. Karteri, Pincer Type Ditertiary Aminomethylphosphine-Pd(II) Complexes Supported on Multi-Walled Carbon Nanotube: catalytic Properties in Heck C-C Coupling Reactions, J. Inorg. Organomet. Polym. Mater. 27 (2017) 138–145, doi:10.1007/s10904-017-0642-5.
[13] S. Uruş, H. Adıgüzel, M. Keleş, İ. Karteri, Multi-walled carbon nanotube supported aminomethylphosphine-Ru(II) complexes: optical behavior and catalytic properties in transfer hydrogenation of acetophenone derivatives, Fullerenes Nanotub. Carbon Nanostructures. 25 (2017) 133–141, doi:10.1080/1536383X.2016.1271789.
[14] S. Uruş, O. Serindağ, M. Diğrak, Synthesis, characterization, and antimicrobial activities of Cu(I), Ag(I), Au(I), and Co(II) complexes with [CH3N(CH2PPh 2)2], Heteroat. Chem 16 (2005) 484–491, doi:10.1002/hc.20145.
[15] S. Uruş, M. Keleş, O. Serindağ, Catalytic synthesis of 2-methyl-1,4-naphthoquinone (vitamin K3) over silica-supported aminomethyl phosphine-Ru(II), Pd(II), and Co(II) complexes, Phosphorus, Sulfur Silicon Relat. Elem. 185 (2010) 1416–1424, doi:10.1080/10426500903061533.
[16] S.W. Zhang, G.B. Zhang, L.P. Lu, Y.S. Li, Novel vanadium(III) complexes with tridentate phenoxy-phosphine [O,P(=O),O] ligands: synthesis, characterization, and catalytic behavior of ethylene polymerization and copolymerization with 10-undecen-1-ol, J. Polym. Sci. Part A Polym. Chem. 51 (2013) 844–854, doi:10.1002/pola.26441.
[17] M. Keleş, T. Keleş, O. Serindağ, S. Yaşar, I. Özdemir, Hydrogenation of acetophenone and its derivatives with 2-propanol using aminomethylphosphine-ruthenium catalysis, Phosphorus, Sulfur Silicon Relat. Elem. 185 (2010) 165–170, doi:10.1080/10426500902754278.
[18] P.E. Garrou, Δr Ring Contributions to 31P NMR Parameters of Transition-Metal-Phosphorus Chelate Complexes, Chem. Rev. 81 (1981) 229–266, doi:10.1021/cr00043a002.
[19] M.I. García-Seijo, A. Habtemariam, P.D.S. Murdoch, R.O. Gould, M.E. García-Fernández, Five-coordinate aminophosphine platinum(II) complexes containing cysteine derivatives as ligands, Inorganica Chim. Acta. 335 (2002) 52–60, doi:10.1016/S0020-1693(02)00813-7.
[20] K. Yashio, M. Kawahata, H. Danjo, K. Yamaguchi, M. Nakamura, T. Imamoto, Construction of optically active multimetallic systems of rhodium(I), palladium(II), and ruthenium(II) with a P-chiral tetraphosphine ligand, J. Organomet. Chem. 694 (2009) 97–102, doi:10.1016/j.jorganchem.2008.10.014.
[21] R. Münzenberg, P. Rademacher, R. Boese, Chiral platinum (II) complexes with phosphorus derivatives of the amino acid L-proline. NMR spectroscopic and X-ray structure investigations of the cis influence of tertiary phosphorus ligands, J. Mol. Struct. 444 (1998) 77–90, doi:10.1016/S0022-2860(97)00308-6.
[22] A. Cavarzan, G. Bianchini, P. Sgarbossa, L. Lefort, S. Gladiali, A. Scarso, G. Strukul, Catalytic asymmetric Baeyer-Villiger oxidation in water by using Pt IIcatalysts and hydrogen peroxide: supramolecular control of enantioselectivity, Chem. - A Eur. J. 15 (2009) 7930–7939, doi:10.1002/chem.200900294.
[23] S. Urus, Synthesis of Fe3O4@SiO2@OSi(CH2)3NHRN(CH2PPh2)2PdCl2 type nanocomposite complexes : highly efficient and magnetically-recoverable catalysts in vitamin K 3 synthesis, 213 (2016) 336–343. https://doi.org/10.1016/j.foodchem.2016.06.093.
[24] H. Tombuloglu, Y. Slimani, G. Tombuloglu, M. Almessiere, A. Baykal, Uptake and translocation of magnetite (Fe3O4) nanoparticles and its impact on photosynthetic genes in barley (Hordeum vulgare L.), Chemosphere 226 (2019) 110–122, doi:10.1016/j.chemosphere.2019.03.075.
[25] Y. Slimani, B. Unal, E. Hannachi, A. Selmi, M.A. Almessiere, M. Nawaz, A. Baykal, I. Ercan, M. Yildiz, Frequency and dc bias voltage dependent dielectric properties and electrical conductivity of BaTiO 3 [sbnd]SrTiO 3 /(SiO 2) x nanocomposites, Ceram. Int. 45 (2019) 11989–12000, doi:10.1016/j.ceramint.2019.03.092.
[26] A. Manikandan, M. Yogasundari, K. Thanrasu, A. Dinesh, K.K. Raja, Y. Slimani, S.K. Jaganathan, R. Srinivasan, A. Baykal, Structural, morphological and optical properties of multifunctional magnetic-luminescent ZnO@Fe3O4 nanocomposite, Phys. E Low-Dimensional Syst. Nanostructures. 124 (2020) 114291, doi:10.1016/j.physe.2020.114291.
[27] F. Absalan, M. Nikazar, Application of Response Surface Methodology for Optimization of Water Treatment by Fe3O4/SiO2/TiO2 Core-Shell Nano-Photocatalyst, Chem. Eng. Commun. 203 (2016) 1523–1531, doi:10.1080/00986445.2016.1218335.
[28] I. Karteri, S. Uruş, H. Özerli, Ş. Karataş, Photovoltaic Performance Photodiodes Based on Reduced Graphene Oxide-Fe3O4 and Carbon Nanotube-Fe3O4 Nanocomposites, Mater. Today Proc. 3 (2016) 1297–1302, doi:10.1016/j.matpr.2016.03.074.
[29] M. Esmaeilpour, J. Javidi, F.N. Dodeji, M.M. Abarghoui, M(II) Schiff base complexes (M = zinc, manganese, cadmium, cobalt, copper, nickel, iron, and palladium) supported on superparamagnetic Fe3O4@SiO2 nanoparticles: synthesis, characterization and catalytic activity for Sonogashira-Hagihara coupling reactions, Transit. Met. Chem. 39 (2014) 797–809, doi:10.1007/s11243-014-9862-5.
[30] J. Zhang, S. Zhai, S. Li, Z. Xiao, Y. Song, Q. An, G. Tian, Pb(II) removal of Fe3O4@SiO2-NH2 core-shell nanomaterials prepared via a controllable sol-gel process, Chem. Eng. J. 215-216 (2013) 461–471, doi:10.1016/j.cej.2012.11.043.
[31] F. Dehghani, A.R. Sardarian, M. Esmaeilpour, Salen complex of Cu(II) supported on superparamagnetic Fe3O 4@SiO2 nanoparticles: an efficient and recyclable catalyst for synthesis of 1- and 5-substituted 1H-tetrazoles, J. Organomet. Chem. 743 (2013) 87–96, doi:10.1016/j.jorganchem.2013.06.019.
[32] M. Esmaeilpour, A.R. Sardarian, J. Javidi, Schiff base complex of metal ions supported on superparamagnetic Fe 3O4@SiO2 nanoparticles: an efficient, selective and recyclable catalyst for synthesis of 1,1-diacetates from aldehydes under solvent-free conditions, Appl. Catal. A Gen. 445-446 (2012) 359–367, doi:10.1016/j.apcata.2012.09.010.
[33] T. Ikariya, Bifunctional Transition Metal-Based Molecular Catalysts for Asymmetric Syntheses, Top Organomet Chem (2011) 31–53, doi:10.1007/3418_2011_2.
[34] S.E. Clapham, A. Hadzovic, R.H. Morris, Mechanisms of the H2-hydrogenation and transfer hydrogenation of polar bonds catalyzed by ruthenium hydride complexes, Coord. Chem. Rev. 248 (2004) 2201–2237, doi:10.1016/j.ccr.2004.04.007.

[35] E.T. Denisov, O.M. Sarkisov, G.I. Likhtenshtein, Catalysis by metal complexes, Chem. Kinet. (2003) 472–501, doi:10.1016/b978-044450938-3/50039-9.
[36] E. Crezee, B.W. Hoffer, R.J. Berger, M. Makkee, F. Kapteijn, J.A. Moulijn, Three-phase hydrogenation of D-glucose over a carbon supported ruthenium catalyst - Mass transfer and kinetics, Appl. Catal. A Gen. 251 (2003) 1–17, doi:10.1016/S0926-860X(03)00587-8.
[37] A. Romero, E. Alonso, Á. Sastre, A. Nieto-Márquez, Conversion of biomass into sorbitol: cellulose hydrolysis on MCM-48 and D-Glucose hydrogenation on Ru/MCM-48, Microporous Mesoporous Mater 224 (2016) 1–8, doi:10.1016/j.micromeso.2015.11.013.
[38] A.A. Dabbawala, D.K. Mishra, J.S. Hwang, Selective hydrogenation of D-glucose using amine functionalized nanoporous polymer supported Ru nanoparticles based catalyst, Catal. Today. 265 (2016) 163–173, doi:10.1016/j.cattod.2015.09.045.
[39] A. Aho, S. Roggan, O.A. Simakova, T. Salmi, D.Y. Murzin, Structure sensitivity in catalytic hydrogenation of glucose over ruthenium, Catal. Today. 241 (2015) 195–199, doi:10.1016/j.cattod.2013.12.031.
[40] D.K. Mishra, J.M. Lee, J.S. Chang, J.S. Hwang, Liquid phase hydrogenation of D-glucose to d-sorbitol over the catalyst (Ru/NiO-TiO 2) of ruthenium on a NiO-modified TiO 2 support, Catal. Today. 185 (2012) 104–108, doi:10.1016/j.cattod.2011.11.020.
[41] J. Zhang, S. Xu, S. Wu, Y. Liu, Hydrogenation of fructose over magnetic catalyst derived from hydrotalcite precursor, Chem. Eng. Sci. 99 (2013) 171–176, doi:10.1016/j.ces.2013.06.002.
[42] E.M. Sulman, M.E. Grigorev, V.Y. Doluda, J. Wärnå, V.G. Matveeva, T. Salmi, D.Y. Murzin, Maltose hydrogenation over ruthenium nanoparticles impregnated in hypercrosslinked polystyrene, Chem. Eng. J. 282 (2015) 37–44, doi:10.1016/j.cej.2015.04.002.
[43] M. Aydemir, A. Baysal, B. Gümgüm, A modular design of metal catalysts for the transfer hydrogenation of aromatic ketones, Appl. Organomet. Chem. 26 (2012) 1–8, doi:10.1002/aoc.1853.
[44] H. Türkmen, Synthesis of 2-aminomethylpiperidine ruthenium(II) phosphine complexes and their applications in transfer hydrogenation of aryl ketones, Appl. Organomet. Chem. 26 (2012) 731–735, doi:10.1002/aoc.2924.
[45] M. Keleş, C. Şahinoğlu, D.M. Emir, M. Mart, New iminophosphine-Ru(II) complexes and their application in hydrogenation and transfer hydrogenation, Appl. Organomet. Chem. 28 (2014) 768–772, doi:10.1002/aoc.3196.
[46] X. Zhu, D. Hou, H. Tao, M. Li, Simply synthesized N-doped carbon supporting Fe3O4 nanocomposite for high performance supercapacitor, J. Alloys Compd. 821 (2020) 153580, doi:10.1016/j.jallcom.2019.153580.
[47] X. Lv, W. Huang, X. Ding, J. He, Q. Huang, J. Tan, H. Cheng, J. Feng, L. Li, Preparation and Photocatalytic Activity of Fe3O4@SiO2@ZnO:la, J. Rare Earths. (2020), doi:10.1016/j.jre.2020.04.007.
[48] A. Kocyigit, I. Orak, İ. Karteri, S. Uruş, The structural analysis of MWCNT-SiO2 and electrical properties on device application, Curr. Appl. Phys. 17 (2017) 1215–1222, doi:10.1016/J.CAP.2017.05.006.
[49] A.G. Orpen, N.G. Connelly, Structural systematics: the role of P-A .sigma.* orbitals in metal-phosphorus .pi.-bonding in redox-related pairs of M-PA3 complexes (A = R, Ar, OR; R = alkyl), Organometallics 9 (1990) 1206–1210, doi:10.1021/om00118a048.
[50] D.G. Gilheany, No d Orbitals but Walsh Diagrams and Maybe Banana Bonds: chemical Bonding in Phosphines, Phosphine Oxides, and Phosphonium Ylides, Chem. Rev. 94 (1994) 1339–1374, doi:10.1021/cr00029a008.
[51] A. Ghosh, C. Kulsi, D. Banerjee, A. Mondal, Galvanic synthesis of Cu2-XSe thin films and their photocatalytic and thermoelectric properties Applied Surface Science Galvanic synthesis of Cu 2 − X Se thin films and their photocatalytic and thermoelectric properties, Appl. Surf. Sci. 369 (2016) 525–534, doi:10.1016/j.apsusc.2016.02.020.
[52] Z. Liu, X. Wang, Q. Cai, C. Ma, Z. Tong, CaBi6O10: a novel promising photoanode for photoelectrochemical water oxidation, J. Mater. Chem. A Mater. Energy Sustain. 5 (2017) 8545–8554, doi:10.1039/C7TA01875D.
[53] M. Diantoro, U. Sa, A. Hidayat, Effect of SnO 2 Nanoparticles on Band Gap Energy of x (SnO 2) -y (Ag) -β- Carotene /FTO Thin Film Effect of SnO 2 Nanoparticles on Band Gap Energy of x (SnO 2) - y (Ag) - β -Carotene /, FTO Thin Film, 2018.
[54] J. Shah, R.K. Kotnala, Rapid green synthesis of ZnO nanoparticles using a hydroelectric cell without an electrolyte Rapid green synthesis of ZnO nanoparticles using a hydroelectric cell without an electrolyte, J. Phys. Chem. Solids. 108 (2017) 15–20, doi:10.1016/j.jpcs.2017.04.007.
[55] A. Rufus, N. Sreeju, D. Philip, RSC Advances applications, RSC Adv. 6 (2016) 94206–94217, doi:10.1039/C6RA20240C.
[56] A. Nikmah, A. Taufiq, A. Hidayat, Synthesis and Characterization of Fe3O4/SiO2 nanocomposites, IOP Conf. Ser. Earth Environ. Sci. (2019) 276, doi:10.1088/1755-1315/276/1/012046.
[57] T. Ikariya, K. Murata, R. Noyori, Bifunctional transition metal-based molecular catalysts for asymmetric syntheses, Org. Biomol. Chem. 4 (2006) 393–406, doi:10.1039/b513564h.
[58] P.A. Lazaridis, S. Karakoulia, A. Delimitis, S.M. Coman, V.I. Parvulescu, K.S. Triantafyllidis, D-Glucose hydrogenation/hydrogenolysis reactions on noble metal (Ru, Pt)/activated carbon supported catalysts, Catal. Today. 257 (2015) 281–290, doi:10.1016/j.cattod.2014.12.006.
[59] D.K. Mishra, A.A. Dabbawala, J.J. Park, S.H. Jhung, J.S. Hwang, Selective hydrogenation of D-glucose to d-sorbitol over HY zeolite supported ruthenium nanoparticles catalysts, Catal. Today. 232 (2014) 99–107, doi:10.1016/j.cattod.2013.10.018.
[60] A. Romero, A. Nieto-Márquez, E. Alonso, Bimetallic Ru, Ni/MCM-48 catalysts for the effective hydrogenation of D-glucose into sorbitol, Appl. Catal. A Gen. 529 (2017) 49–59, doi:10.1016/j.apcata.2016.10.018.
[61] B.W. Hoffer, E. Crezee, F. Devred, P.R.M. Mooijman, W.G. Sloof, P.J. Kooyman, A.D. Van Langeveld, F. Kapteijn, J.A. Moulijn, The role of the active phase of Raney-type Ni catalysts in the selective hydrogenation of D-glucose to D-sorbitol, Appl. Catal. A Gen. 253 (2003) 437–452, doi:10.1016/S0926-860X(03)00553-2.
[62] S. Rajagopal, RuC12 (PPh3), -catalyzed transfer hydrogenation of d-glucose, 75 (1992).
[63] Z. Li, Y. Liu, S. Wu, Efficient conversion of D-glucose into D-sorbitol over carbonized cassava dregs-supported ruthenium nanoparticles catalysts, Bioresources 13 (2018) 1278–1288, doi:10.15376/biores.13.1.1278-1288.
[64] B. García, J. Moreno, G. Morales, J.A. Melero, J. Iglesias, Production of sorbitol via catalytic transfer hydrogenation of Glucose, Appl. Sci. (2020) 10, doi:10.3390/app10051843.
[65] B. Baruwati, V. Polshettiwar, R.S. Varma, Magnetically recoverable supported ruthenium catalyst for hydrogenation of alkynes and transfer hydrogenation of carbonyl compounds, Tetrahedron Lett 50 (2009) 1215–1218, doi:10.1016/j.tetlet.2009.01.014.